

## Assessment of a quantitative metric for 4D CT artifact evaluation by observer consensus

Sarah J. Castillo,<sup>1,2a</sup> Richard Castillo,<sup>1,2</sup> Peter Balter,<sup>1,2</sup> Tinsu Pan,<sup>1,3</sup> Geoffrey Ibbott,<sup>1,2</sup> Brian Hobbs,<sup>1,4</sup> Ying Yuan,<sup>1,4</sup> and Thomas Guerrero<sup>1,2,5</sup>  
*The University of Texas Health Science Center,<sup>1</sup> Houston, TX; Divisions of Radiation Oncology,<sup>2</sup> Diagnostic Imaging,<sup>3</sup> and Quantitative Sciences,<sup>4</sup> The University of Texas MD Anderson Cancer Center, Houston, TX; Department of Computational and Applied Mathematics,<sup>5</sup> Rice University, Houston, TX, USA*  
sjoy@mdanderson.org

Received 16 September, 2013; accepted 6 January, 2014

The benefits of four-dimensional computed tomography (4D CT) are limited by the presence of artifacts that remain difficult to quantify. A correlation-based metric previously proposed for ciné 4D CT artifact identification was further validated as an independent artifact evaluator by using a novel qualitative assessment featuring a group of observers reaching a consensus decision on artifact location and magnitude. The consensus group evaluated ten ciné 4D CT scans for artifacts over each breathing phase of coronal lung views assuming one artifact per couch location. Each artifact was assigned a magnitude score of 1–5, 1 indicating lowest severity and 5 indicating highest severity. Consensus group results served as the ground truth for assessment of the correlation metric. The ten patients were split into two cohorts; cohort 1 generated an artifact identification threshold derived from receiver operating characteristic analysis using the Youden Index, while cohort 2 generated sensitivity and specificity values from application of the artifact threshold. The Pearson correlation coefficient was calculated between the correlation metric values and the consensus group scores for both cohorts. The average sensitivity and specificity values found with application of the artifact threshold were 0.703 and 0.476, respectively. The correlation coefficients of artifact magnitudes for cohort 1 and 2 were 0.80 and 0.61, respectively, ( $p < 0.001$  for both); these correlation coefficients included a few scans with only two of the five possible magnitude scores. Artifact incidence was associated with breathing phase ( $p < 0.002$ ), with presentation less likely near maximum exhale. Overall, the correlation metric allowed accurate and automated artifact identification. The consensus group evaluation resulted in efficient qualitative scoring, reduced interobserver variation, and provided consistent identification of artifact location and magnitudes.

PACS numbers: 87.57.qp, 87.55.Gh, 87.57.C-

Key words: 4D CT, artifacts, correlation, visual assessment

### I. INTRODUCTION

Four-dimensional computed tomography (4D CT) is a common method of radiation therapy simulation used to account for respiratory motion in treatment planning.<sup>(1–5)</sup> Four-dimensional CT has allowed reduction of motion artifacts and systematic uncertainty in treatment planning, enabling smaller target margins.<sup>(6–9)</sup> Two implementations of 4D CT are commonly used: ciné 4D CT<sup>(10,11)</sup> and helical 4D CT.<sup>(8,11,12)</sup>

<sup>a</sup> Corresponding author: Sarah J. Castillo, The University of Texas MD Anderson Cancer Center, 1515 Holcombe Blvd., Unit 97, Houston TX 77030, USA; phone: 713-745-2407; fax: 713-563-2545; email: sjoy@mdanderson.org

Ciné 4D CT is an axial mode of CT that acquires discrete segments of multislice images across the scan extent, while helical 4D CT uses a low pitch across the scan extent. Each implementation ideally acquires each imaged voxel for at least one breathing cycle. Breathing information is derived from an independent external surrogate for internal motion that provides a one-dimensional respiratory trace during image acquisition. This allows images to be sorted into multiple, typically ten, 3D CT scans, each representing a breathing phase. This study focused on ciné 4D CT, which sorts phases on the basis of a nearest-neighbor technique, typically phase sorting, that finds the image segment closest in time to each externally derived breathing phase at each couch position.<sup>(2,13)</sup>

The ciné acquisition and phase sorting of discrete image segments often result in coronal and sagittal views that exhibit artifacts (see Fig. 1) in the form of discontinuous bands of image segments between couch positions. Artifacts, or artificial anatomic spatial distributions, cause uncertainty in the true anatomic spatial distribution and errors in anatomic delineation, treatment targeting, and lung function images derived from CT.<sup>(14-19)</sup> Therefore, many studies have explored methods to evaluate and reduce the frequency and magnitude of 4D CT artifacts.

Cui et al.<sup>(20)</sup> devised a correlation metric (CM) for assessment of ciné artifacts that attempts to account for normal anatomic variations. This metric correlates the image slices across two neighboring couch positions and subtracts the average of correlations between adjacent image slices within the neighboring couch positions. This is a straightforward, efficient metric that can potentially distinguish normal anatomic variation from artifact and is very promising. However, the metric's validation was limited to relative metric values between ten 4D CT scans with two observers. Validation of this metric can be improved by a receiver operating characteristic (ROC) analysis<sup>(21,22)</sup> to assess the metric's accuracy in artifact identification.

Han et al.<sup>(23)</sup> also explored use of a correlation metric for artifact indication on helical scans using a reference 'bridge stack' of images overlapping in anatomy at different breathing phases. This method has advantages of automation and efficiency, but requires use of an anatomic reference that is derived from the 4D CT scan and, therefore, subject to the artifacts being attempted to quantify. The current standard of artifact evaluation is manual visual assessment, which is associated with high interobserver variability, lack of quantitative power, and lengthy analysis times. A consensus group of expert observers may reduce analysis times and interobserver variation, yielding a higher quality standard evaluation dataset.

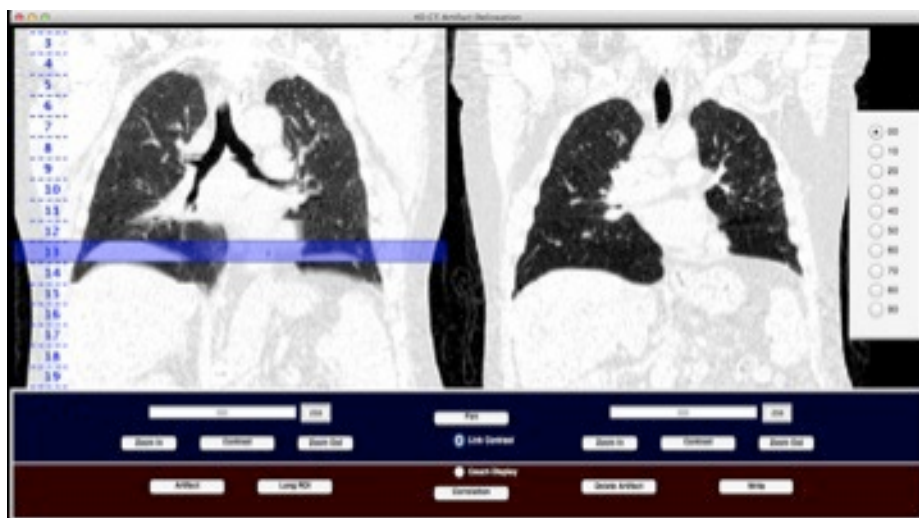


FIG. 1. Artifact evaluation software showing: T0% of a 4D CT scan (left) with a highlighted identified artifact at couch position 13 indicating a saved artifact location; and corresponding deep-inspiration breath-hold scan (right) used as an anatomic reference for artifact identification in the 4D CT (left).

In this study, a consensus group evaluated ciné artifacts in ten 4D CT scans to form a standard dataset. This dataset was then used to assess the performance of the correlation metric in artifact identification<sup>(20)</sup> through ROC analysis.

## II. MATERIALS AND METHODS

### A. The proposed metric

The metric proposed by Cui et al.<sup>(20)</sup> is based on a normalized cross-correlation (NCC) coefficient between two axial images (Eq. (1)). This coefficient is commonly used in template matching to determine the position of a given pattern in an image.<sup>(24)</sup> The position of a template  $t$  within an image  $f(x,y)$  is given by  $(u,v)$ , where  $\bar{t}$  is the mean of the template pixel intensities and  $\bar{f}_{u,v}$  is the mean of  $f(x,y)$  pixel intensities in the region under the template. The maximum NCC value gives the position match.

$$NCC = \frac{\sum_{x,y} [(f(x,y) - \bar{f}_{u,v})(t(x-u, y-v) - \bar{t})]}{(\sum_{x,y} [f(x,y) - \bar{f}_{u,v}]^2 \sum_{x,y} [t(x-u, y-v) - \bar{t}]^2)^{0.5}} \quad (1)$$

The Pearson correlation coefficient  $C$  is typically used in correlation studies to assess a linear relationship between two variables or images. The two-dimensional (2D) Pearson correlation coefficient was used in this study (Eq. (2)) for efficiency of correlating an image A with a second image B, where  $\bar{A}$  is the mean of image A pixel intensities,  $\bar{B}$  is the mean of image B pixel intensities, and  $(m,n)$  are indices of pixel rows and columns, respectively. The Pearson correlation coefficient  $C$  is equal to the maximum NCC coefficient when the two images are properly aligned. We chose to use the Pearson correlation coefficient rather than the NCC coefficient because the Pearson correlation coefficient requires less computation time and is more intuitively understood.

$$C = \frac{\sum_m \sum_n (A_{mn} - \bar{A})(B_{mn} - \bar{B})}{\sqrt{(\sum_m \sum_n (A_{mn} - \bar{A})^2)(\sum_m \sum_n (B_{mn} - \bar{B})^2)}} \quad (2)$$

All calculations were performed using MATLAB (The MathWorks, Inc., Natick, MA) with the *corr2* function (Eq. (2)) for the correlations. The correlation metric devised by Cui et al.<sup>(20)</sup> (Eq. (3)) was calculated between each couch position  $N$  per breathing phase per 4D CT scan. A couch position is a reference to a beam-width size superior–inferior location across the scan extent; each couch position contains a sorted image segment with  $8 \times 2.5$  mm thick axial images. The Pearson correlation coefficient  $C$  was calculated between image 7 and image 8 of couch position  $N$  ( $C_{7,8}^N$ ), then between image 1 and image 2 of the inferior couch position  $N+1$  ( $C_{1,2}^{N+1}$ ); the resulting two coefficients were averaged to account for normal anatomic variation. The coefficient between image 8 of couch position  $N$  and image 1 of couch position  $N+1$  ( $C_{8,1}^{N,N+1}$ ) was subtracted from this average, yielding final metric CM. A lower CM value indicates a better image match, and a lower artifact severity. Each 4D CT scan had a corresponding matrix of  $((N_T - 1) \times 10)$  CM values, where  $N_T$  is the total number of couch positions per each of 10 phases.

$$CM = 0.5(C_{7,8}^N + C_{1,2}^{N+1}) - C_{8,1}^{N,N+1} \quad (3)$$

One metric per each couch position 2 through  $N_T - 1$  was needed for comparison with observer results, so each couch position's bordering CM values were averaged to mimic how an observer would assess a couch position for artifact presence. A final normalized correlation metric (NCM) was calculated by dividing each CM value by the average of CM values within that phase. This normalization allowed retention of the relative values for comparison between 4D CT scans and between phases, while yielding a common reference point for 4D CT scans.

### B. The sample evaluated

We identified ten patients scheduled to undergo thoracic radiation therapy at our institution. Our study sample consisted of the clinical ciné 4D CT scans used for each identified patient's radiation treatment plan. All 4D CT images were acquired using a GE Discovery ST PET/CT scanner (GE Medical Systems, Waukesha, WI), with the 8-slice LightSpeed CT component, and retrospectively reviewed. All image segments were  $8 \times 2.5$  mm slices with an x and y voxel size of 0.97 mm. Phases were binned evenly in time between user-defined maximum inhalation peaks for all cases. Maximum inhale is represented by T0%, with each subsequent breathing phase per cycle defined in 10% increments of the breathing period for that cycle (i.e., T0%, T10%, T20%, etc.). All 4D CT scans were phase-sorted with this binning technique using the GE Advantage Workstation software (GE Medical Systems).

A sample size calculation estimated the minimal number of 4D CT scans necessary for metric evaluation. Two cohorts were needed, one to determine a metric threshold for artifact identification and a second to evaluate the determined artifact threshold. We calculated an exact test for single proportion (Eq. (4)) to determine the sample size with the software nQuery Advisor (Statistical Solutions, Boston, MA). Given x successes out of n trials,  $x = 0, 1, \dots, n$ , the p-value for an exact, two-sided binomial test under null success rate  $\phi_0$  is computed by summing the probability of observing values of the sample space that are as or more extreme than x.

$$\sum_{u=0}^x \frac{n!}{u!(n-u)!} \pi_0^u (1-\pi_0)^{n-u} + \sum_{u=n-x+1}^n \frac{n!}{u!(n-u)!} \pi_0^u (1-\pi_0)^{n-u} \quad (4)$$

A test significance alpha level of 0.1 was used with type 1 error and a power of 0.81. A two-sided null hypothesis of 0.5 with an alternative of 0.75 was chosen, indicating the metric could not definitively identify an artifact or that it could identify at least three artifacts of every four artifacts present. This yielded 26 artifacts needed per cohort. If at least one artifact exists per breathing phase per 4D CT scan, then a single 4D CT scan will contain at least ten artifacts. Therefore, five 4D CT scans per cohort were evaluated, approximately double the number of artifacts needed. Each 4D CT scan was briefly visually assessed to ensure this minimum artifact requirement was met.

### C. Observer artifact assessment

Thorough visual assessment is time-consuming and associated with high interobserver variance,<sup>(25)</sup> but remains the standard artifact evaluation method. To reduce both the time required and interobserver variance, we organized a committee of observers to view images simultaneously and reach a consensus on artifact location and magnitude. We termed this committee the consensus group. The consensus group consisted of a physician specializing in thoracic oncology, a physics assistant working with ciné 4D CT, two physicists in the thoracic service, and a dosimetrist who works with thoracic treatment plans. An independent member, a graduate student studying 4D CT, coordinated each assessment and distributed materials necessary for evaluation, but did not participate in the actual assessment.

Prior to the first consensus group meeting, instructions for artifact evaluation were given to all consensus group members. The same instructions were provided at each consensus group meeting. The instructions included definitions and examples of ciné 4D CT artifacts with our magnitude scoring system, as well as an example of a cardiac artifact that results from the

heart beating asynchronously from the breathing motion of the lung that may potentially be mistaken for a 4D CT artifact. These instructions served as a baseline reference to calibrate each observer's visual scale.

If a couch position within a breathing phase was identified as containing an artifact, it was assumed that the identified artifact existed at all image slices at that couch position within that phase. All couch positions covering lung anatomy were assessed; couch positions below the displayed inferior lung were considered in assessment if there appeared to be an artifact at that location interfering with display of what should have been the most inferior lung anatomy. Each identified artifact was assigned a magnitude score between 1 and 5, with 1 indicating an artifact with a minor degree of interference with true anatomy and 5 indicating a large degree of interference with true anatomy; Fig. 2 gives an example of artifact scores assigned. Coronal views were assessed in all 10 phases of each patient. A helical deep-inspiration, breath-hold scan acquired within the same examination as the 4D CT scan was displayed next to the 4D CT scan during assessment to serve as an anatomic reference as it is free of the ciné 4D CT artifacts being evaluated. Artifacts were assessed using custom MATLAB software that allowed simultaneous coronal display of a component breathing phase of the 4D CT and the coronal display of the breath-hold. This software also allowed the ability to scroll through the images, change the window and level, zoom in or out, display the couch position locations, change the breathing phase, and save identified artifact's corresponding couch position and score (Fig. 1).

Before the 4D CT evaluation, a lung window of level -450 HU and window 1100 HU was set for both the breath-hold scan and the 4D CT scan. Each was zoomed so that the entire lung with an extra couple of surrounding couch positions could be viewed. The couch positions of the 4D CT scan were displayed after the zoom so that observers could identify correct couch positions. Two sets of numbered cards were distributed to each observer, and the observers used these cards to identify couch positions and scores for artifacts independent of the other observers' choices.

The breath-hold scan was scrolled through before each 4D CT evaluation for anatomic reference, and then the entire lung in the selected 4D CT breathing phase was scrolled through, allowing time for observers to choose their numbered cards for artifact location and score. Then for each couch position within the lung, the consensus group was asked if the stated couch position contained an artifact. Each observer shared the numbered cards he or she had chosen. Results were saved if all consensus members agreed on an artifact location and score; if different answers were chosen, the observers made a case for their reasoning and the images were reviewed until the group achieved a consensus. Only rarely was no consensus reached; in these cases the majority ruled.

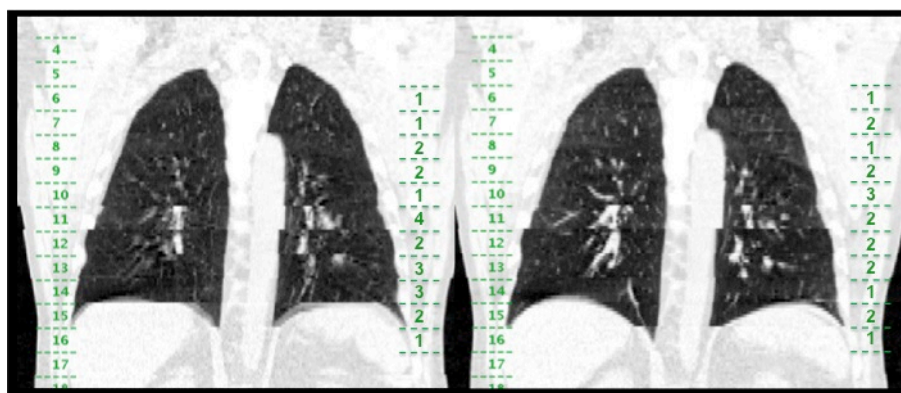


FIG. 2. Example of coronal slices taken from T10% (left) and T90% (right) of patient C2\_1 (NCM values shown in Fig. 3.), with couch positions indicated on the left side of each coronal view and consensus group identified scores per couch position shown on the right side of each coronal view. The artifact in T10% at couch position 11 was scored as a more severe artifact based on the higher interference of the artifact with anatomy.

### C.1 Statistical analysis of observer artifact assessment

A logistic mixed effects model was used to evaluate the relationship between artifact incidence and breathing phase from consensus results from all ten patient cases using the lme4 package in R.2.14.0 (<http://www.r-project.org/>). The utilized mixed logistic model facilitates joint estimation of the log-odds of artifact incidence across all phases, while accounting for the inherent correlation among observations derived from the same patient scan, to estimate and characterize the extent of variability associated with breathing phase. The likelihood ratio test for association is reported; this test is used to weigh the observed evidence of homogeneity (i.e., the identical log-odds for all phases). In addition, phase effects were evaluated for significance using two-sided Wald tests. Wald tests are used to weigh the observed evidence of phase-specific log-odds adjustments from component phase T0% in the presence of the estimated within and between subject sources of variability. Post hoc application of the sequentially rejective Bonferroni method was used to adjust p-values for multiple comparisons of the adjustments of log-odds of artifact incidence from component phase T0% across phases T10% through T90%.<sup>(26)</sup> The multiple phase comparisons inflate the nominal false positive rate, and thus p-values need to be adjusted to maintain the type I error rate at 5%.

### D. Artifact threshold derivation and evaluation

An ROC method was used to determine an artifact threshold with cohort 1; this artifact threshold was then applied to cohort 2 for evaluation of resulting sensitivity and specificity. The artifact threshold is a NCM value. A 4D CT contains NCM values for each component breathing phase at each couch position except the first and last as given in the matrix  $((N_T-2) \times 10)$ . The NCM values above or equal to the applied artifact threshold value will indicate an artifact at an anatomic location (N) and breathing phase. MATLAB software was developed to format observer results and produce ROC curves. In order to generate ROC curves, a binary decision threshold is moved across the data, above which an artifact is identified, below which an artifact is not identified; each decision threshold yields a sensitivity and false-positive fraction point on the curve.<sup>(27)</sup> The decision threshold was incremented by 1% between the minimum NCM value and the maximum NCM value contained within each cohort 1 patient  $((N_T-2) \times 10)$  matrix. As the decision threshold was incremented, NCM values below the decision threshold were set to zero, indicating no artifact presence. The consensus results served as the ground truth to determine the true-positive fraction, true-negative fraction, false-positive fraction, and false-negative fraction.

Parameters were calculated from the ROC curves to assess the accuracy of the NCM and find the resultant artifact threshold. For each patient in cohort 1, the area under the curve (AUC) was calculated to determine the NCM accuracy, and the Youden index was calculated to extract a threshold. The Youden index J is the maximum vertical distance between the ROC curve and the diagonal “chance line”, which can also be related back to a decision threshold point directly (Eq. (5)).

$$J = \max(sensitivity(dc) + specificity(dc) - 1) \quad (5)$$

The Youden index represents the optimal cut-point in ROC curve analysis and is used as another measure of accuracy. Youden's index values vary between 0 and 1, with 1 indicating a relatively large NCM evaluation accuracy.<sup>(28)</sup> The artifact threshold was derived from the Youden index to provide the optimal artifact threshold corresponding to maximum accuracy in each ROC curve. The point in the curve at which the Youden index was found yielded the corresponding NCM threshold.

The artifact threshold corresponding to the minimum Youden index found in cohort 1 was taken as the final artifact threshold. One outlier index existed, and thus an average of thresholds was deemed inappropriate, and the minimum was taken to ensure that artifacts would not be missed. The determined artifact threshold was applied to each  $((N_T-2) \times 10)$  matrix of NCM

values in cohort 2. All cohort 1 ROC curves and parameters, and cohort 2 sensitivity and specificity values were calculated using consensus group results as the ground truth.

#### E. Relationship between artifact magnitudes and metric values

To evaluate whether the relative NCM values accurately reflected the degree of artifact severity, or artifact magnitude, the artifact score for each consensus group-identified artifact among all ten cases was compared to the NCM value corresponding to the couch position and breathing phase of that artifact score. A Pearson correlation coefficient and a p-value were calculated for each patient.

### III. RESULTS

#### A. Metric

Evaluated cases are labeled first by the cohort (C1 or C2) followed by a number indicating the order of evaluation within that cohort. An example of NCM values over all couch positions for 2 component phases for the first patient of cohort 2, C2\_1, is shown in Fig. 3; coronal image slices from the same 2 component phases of the C2\_1 case are also shown in Fig. 2 for comparison to Fig. 3 and for an example of consensus-chosen scores.

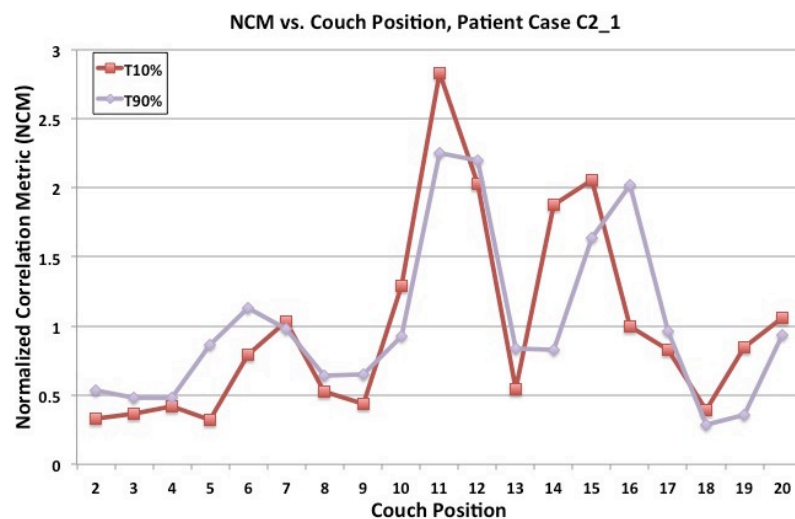


FIG. 3. Normalized correlation metric (NCM) vs. couch positions for patient case C2\_1. Breathing phases T10% and T90% are displayed for comparison with coronal views of T10% and T90% in Fig. 2.

### B. Consensus artifact results

The consensus group scored all 10 phases of a 4D CT scan in under 40 minutes, on average within 30 minutes. The mean percentage of couch positions covering lung anatomy that contained consensus-chosen artifacts for both cohorts was 68.7%. The first patient scored by the consensus group had the lowest percentage of lung couch positions containing artifacts: 32.4%; all other patients had artifacts in at least 59% of lung couch positions with a maximum percentage of 87.3%.

Artifact incidence was significantly associated with breathing phase using logistic mixed effects analysis ( $p < 0.002$  likelihood ratio test). The estimated probability of observing an artifact during the T60% phase was significantly lower than T10% (odds ratio = 0.44,  $p < 0.003$ ), T70% (odds ratio = 0.41,  $p < 0.0015$ ), T80% (odds ratio = 0.33,  $p < 0.0002$ ), and T90% (odds ratio = 0.36,  $p < 0.0004$ ) phases after adjusting for multiplicity. Figure 4 demonstrates the model-estimated probability of an artifact at each phase with 95% confidence intervals.

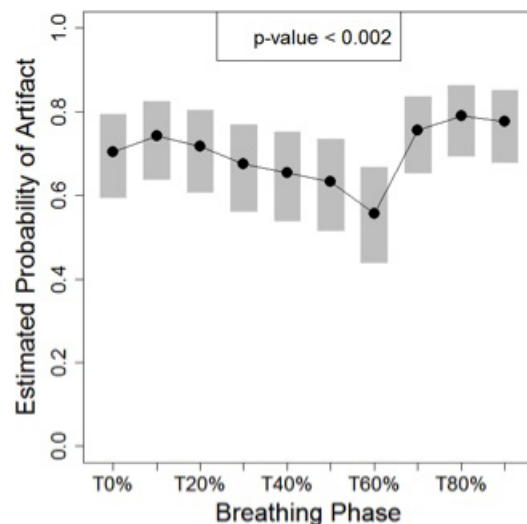


FIG. 4. Estimated probability of artifacts as a function of phase and associated 95% confidence intervals (grey bars). The risk of an artifact decreased for exhale phase images. The p-value derives from the likelihood ratio test of the global null hypothesis of the absence of association with phase.

### C. ROC analysis

Figure 5 demonstrates an example ROC curve generated for case C1\_5 with associated parameters, also listed in Table 1, which displays the ROC curve parameters for each cohort 1 patient. The artifact threshold found using this method was 73%. The average (AVG) cohort 2 sensitivity resulting from the applied artifact threshold of 73% was 0.703, and the average specificity of cohort 2 was 0.476, each with a standard deviation (STD) of 0.11.

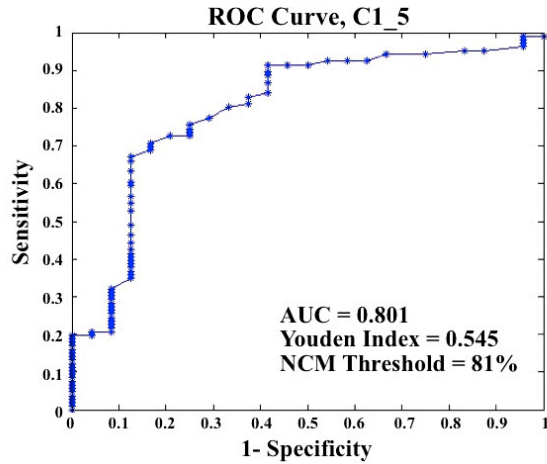


FIG. 5. Example ROC curve from case C1\_5 of cohort 1, with area under the curve (AUC), Youden index, and corresponding NCM threshold indicated.

TABLE 1. Cohort 1 ROC parameters.

Parameter	C1_1	C1_2	C1_3	C1_4	C1_5
AUC (area under curve)	0.756	0.525	0.769	0.709	0.801
Youden's index	0.446	0.103	0.507	0.461	0.545
NCM threshold	125%	73%	93%	93%	81%

#### D. Metric correlation with consensus scores

The mean of cohort 1 Pearson correlation coefficients was 0.80, with all but the first case yielding a coefficient greater than 0.91; the composite correlation coefficient was 0.54. The mean of cohort 2 Pearson correlation coefficients was 0.61, with three of the five cases yielding coefficients greater than 0.99; the composite correlation coefficient was 0.58. The composite p-values for both cohorts were less than 0.001, indicating a nonzero correlation between the NCM and consensus scores.

#### IV. DISCUSSION

We found that the average sensitivity and artifact score correlation achieved for the NCM assessment against the consensus group assessment indicate a moderately high performance of the NCM method for ciné 4D CT artifact evaluation. The sensitivity was high, while the specificity was only moderate, suggesting the artifact threshold found using cohort 1 overestimated the true number of artifact locations. This was expected as we chose the artifact threshold corresponding to the minimum Youden index, the cohort 1 outlier, to favor not missing an artifact at the expense of falsely identifying a position as containing an artifact. However, even with this trade-off, the sensitivity was not as high as expected. This may be due to the inexperience of the consensus group members present with the first few cases. If the consensus group members had participated in a practice session an outlier might have been avoided, and the artifact threshold would have been derived over an average of the sample rather than from the outlier value. Had a larger cohort 1 sample size been evaluated, a decreased outlier detriment would have allowed an average-derived artifact threshold.

The artifact score correlations between the NCM values and consensus results were good on an individual basis, but a few cases with poor coefficients lowered the composite correlation coefficient. The first case had a poor coefficient (0.169) that would have been improved from a practice session to familiarize the observers with the procedure and appropriate scoring system based on the given instructions. The other two cases containing poor coefficients (0.342 and 0.408) did not contain any consensus magnitude scores higher than 2, which left only two data points for the correlation. An increase in cohort 1 sample size may also have provided more cases with scores over the range 1–5 to offset these poor correlations.

This study would have benefited from a practice session to train observers before the consensus evaluations and an increased cohort 1 sample size of patient 4D CT cases to offset the effect of an outlier and provide more data points for artifact score correlation. However, even with these weaknesses, the consensus group method of visual assessment allowed an efficient and guided scoring that produced a high quality research dataset for metric validation, a reduced interobserver variation, and provided a more consistent method of identifying artifact locations and magnitudes. The NCM also performed well despite these issues and resulted in a reproducible automated quantitative evaluation within a time unachievable by observer evaluations; the NCM is also simple to implement as it is based on the Pearson correlation coefficient, and thus would integrate well into the clinical workflow.

The results of the logistic mixed effects analysis demonstrate that artifacts are less likely to be present near exhale. This is intuitive as exhale is a more stable breathing state; passive exhale ends at the functional residual capacity, the equilibrium point between the chest wall expansion and lung contraction. In particular, there was a significant reduction in artifact odds associated with T60% when compared to T10%, T70%, T80%, and T90%. These images were phase-sorted using ten equally divided bins, and did not explicitly define T50% to be maximum exhale. As time from peak inhalation to peak exhalation is typically longer than time from peak exhalation to peak inhalation,<sup>(29)</sup> T60% may have more truly represented maximum exhale than other phases such as T50%, providing an explanation for why only T60% contained a significant artifact reduction.

Currently, visual assessment is the evaluation standard, but it lacks a clear set of rules, which makes extraction of quantitative results difficult. Some visual assessments display example images with a description of the overall artifact presence, whether on an individual basis or as a comparison between scans,<sup>(1,13,30–38)</sup> while others state a particular method of an independent expert evaluation.<sup>(15,39–42)</sup> Our study extracted a quantitative artifact evaluation from qualitative observations in a guided and efficient method that reduced interobserver variability. This yielded a high-quality research dataset for 10 breathing phases of ten patients in approximately 5 hours. This consensus group method of evaluation could also be used for images from various acquisition and processing methods and even for various types of artifacts, as long as instructions on identification and characterization are provided for observer guidance, preferably with a practice session before the first case analysis.

Similar evaluations have been done with images derived from phantoms and software simulations, in which the exact anatomic volume and shape are known.<sup>(31,34,35,43–46)</sup> Persson et al.<sup>(14,47)</sup> evaluated artifacts in terms of gross tumor volume deviations in comparison with a reference target volume. Among other quantitative artifact evaluations exist the following: deviations in target centroid position or contours,<sup>(37,48,49)</sup> the mean square gray value difference between couch positions,<sup>(1)</sup> tidal volume variations from reference images,<sup>(36)</sup> and external surrogate parameters.<sup>(50)</sup> The quantitative metric evaluated in this study offers an efficient, reliable method to evaluate ciné artifact location and magnitude in the lung.

## V. CONCLUSIONS

We conclude that the correlation metric assessed has the potential to be used as a ciné 4D CT artifact evaluator when an efficient and reliable method is needed for processing many sets of images, though additional cases would yield an even more accurate artifact threshold for identification. We also conclude that the consensus group method has the potential to be used as a research standard for evaluating 4D CT artifacts and as a standard to evaluate alternative quantitative artifact evaluation methods, and recommend a consensus practice session before evaluation.

## ACKNOWLEDGMENTS

We thank the members of the consensus group for their time and participation in the study. Financial support for this research was provided by an NIH Director's New Innovator Award (DP2OD007044). RC was partially supported by NIH through a Loan Repayment Program Award and an NCI Mentored Research Scientist Award (K01CA181292).

## REFERENCES

1. Ehrhardt J, Werner R, Saring D, et al. An optical flow based method for improved reconstruction of 4D CT data sets acquired during free breathing. *Med Phys*. 2007;34(2):711–21.
2. Rietzel E, Pan T, Chen GT. Four-dimensional computed tomography: image formation and clinical protocol. *Med Phys*. 2005;32(4):874–89.
3. Low DA, Nystrom M, Kalinin E, et al. A method for the reconstruction of four-dimensional synchronized CT scans acquired during free breathing. *Med Phys*. 2003;30(6):1254–63.
4. Keall PJ, Mageras GS, Balter JM, et al. The management of respiratory motion in radiation oncology. AAPM Report 91. Reprt of the AAPM Task Group 76. College Park, MD: AAPM; 2006.
5. Guckenberger M, Wilbert J, Meyer J, Baier K, Richter A, Flentje M. Is a single respiratory correlated 4d-ct study sufficient for evaluation of breathing motion? *Int J Radiat Oncol Biol Phys*. 2007;67(5):1352–59.
6. Keall PJ, Joshi S, Vedam SS, Siebers JV, Kini VR, Mohan R. Four-dimensional radiotherapy planning for DMLC-based respiratory motion tracking. *Med Phys*. 2005;32(4):942–51.
7. Vedam SS, Kini VR, Keall PJ, Ramakrishnan V, Hostafavi H, Mohan R. Quantifying the predictability of diaphragm motion during respiration with a noninvasive external marker. *Med Phys*. 2003;30(4):505–13.
8. Ford E, Mageras G, York E, Ling CC. Respiration-correlated spiral CT: a method of measuring respiratory-induced anatomic motion for radiation treatment planning. *Med Phys*. 2003;30(1):88–97.
9. Liao ZX, Komaki RR, Thames HD Jr, et al. Influence of technologic advances on outcomes in patients with unresectable, locally advanced non-small-cell lung cancer receiving concomitant chemoradiotherapy. *Int J Radiat Oncol Biol Phys*. 2010;76(3):775–81.
10. Vedam SS, Keall PJ, Kini VR, Mostafavi H, Shukla HP, Mohan R. Acquiring a four-dimensional computed tomography dataset using an external respiratory signal. *Phys Med Biol*. 2003;48(1):45–62.
11. Pan T. Comparison of helical and ciné acquisitions for 4D-CT imaging with multislice CT. *Med Phys*. 2005;32(2):627–34.
12. Keall PJ, Starkschall G, Shukla H, et al. Acquiring 4D thoracic CT scans using a multislice helical method. *Phys Med Biol*. 2004;49(10):2053–67.
13. Rietzel E and Chen GT. Improving retrospective sorting of 4D computed tomography data. *Med Phys*. 2006;33(2):377–79.
14. Persson GF, Nygaard DE, Brink C, et al. Deviations in delineated GTV caused by artefacts in 4DCT. *Radiother Oncol*. 2010;96(1):61–66.
15. Yamamoto T, Langner U, Loo BW Jr, Shen J, Keall PJ. Retrospective analysis of artifacts in four-dimensional CT images of 50 abdominal and thoracic radiotherapy patients. *Int J Radiat Oncol Biol Phys*. 2008;72(4):1250–58.
16. Watkins WT, Li R, Lewis J, et al. Patient-specific motion artifacts in 4DCT. *Med Phys*. 2010;37(6):2855–61.
17. Nakamura M, Narita Y, Sawada A, et al. Impact of motion velocity on four-dimensional target volumes: a phantom study. *Med Phys*. 2009;36(5):1610–17.
18. Louie AV, Rodrigues G, Olsthoorn J, et al. Inter-observer and intra-observer reliability for lung cancer target volume delineation in the 4D-CT era. *Radiother Oncol*. 2010;95(2):166–71.
19. Castillo R, Castillo E, McCurdy M, et al. Spatial correspondence of 4D CT ventilation and SPECT pulmonary perfusion defects in patients with malignant airway stenosis. *Phys Med Biol*. 2012;57(7):1855–71.
20. Cui G, Jew B, Hong JC, Johnston EW, Loo BW Jr, Maxim PG. An automated method for comparing motion artifacts in ciné four-dimensional computed tomography images. *J Appl Clin Med Phys*. 2012;13(6):3838.

21. Hanley JA and McNeil BJ. The meaning and use of the area under a receiver operating characteristic (ROC) curve. *Radiology*. 1982;143(1):29–36.
22. Metz CE. ROC analysis in medical imaging: a tutorial review of the literature. *Radiol Phys Tech*. 2008;1(1):2–12.
23. Han D, Bayouth J, Bhatia S, Sonka M, Wu X. Characterization and identification of spatial artifacts during 4D-CT imaging. *Med Phys*. 2011;38(4):2074–87.
24. Briechle K and Hanebeck UD. Template matching using fast normalized cross correlation. *Proc Soc Photo-Opt Ins*. 2001;4387:95–102.
25. Wei JGL. Quantification of motion artifacts in 4DCT using global Fourier analysis. *Signal Processing in Medicine and Biology Symposium (SPMB)*, 1 December 2012. New York: IEEE; 2012.
26. Proschan MA and Waclawiw MA. Practical guidelines for multiplicity adjustment in clinical trials. *Control Clin Trials*. 2000;21(6):527–39.
27. Bushberg JT, Seibert JA, Leidholdt EM, Boone JM. *The essential physics of medical imaging*, 3rd edition. Philadelphia, PA: Lippincott Williams and Wilkins; 2011.
28. Schisterman EF, Perkins NJ, Liu A, Bondell H. Optimal cut-point and its corresponding Youden Index to discriminate individuals using pooled blood samples. *Epidemiology*. 2005;16(1):73–81.
29. Balter JM, Lam KL, McGinn CJ, Lawrence TS, Ten Haken RK. Improvement of CT-based treatment-planning models of abdominal targets using static exhale imaging. *Int J Radiat Oncol Biol Phys*. 1998;41(4):939–43.
30. Carnes G, Gaede S, Yu E, Van Dyk J, Battista J, Lee TY. A fully automated non-external marker 4D-CT sorting algorithm using a serial ciné scanning protocol. *Phys Med Biol*. 2009;54(7):2049–66.
31. Abdelnour AF, Nehmeh SA, Pan T, et al. Phase and amplitude binning for 4D-CT imaging. *Phys Med Biol*. 2007;52(12):3515–29.
32. Keall PJ, Vedam SS, George R, Williamson JF. Respiratory regularity gated 4D CT acquisition: concepts and proof of principle. *Australas Phys Eng Sci Med*. 2007;30(3):211–20.
33. Pan T, Sun X, Luo D. Improvement of the ciné-CT based 4D-CT imaging. *Med Phys*. 2007;34(11):4499–503.
34. Gianoli C, Riboldi M, Spadea MF, et al. A multiple points method for 4D CT image sorting. *Med Phys*. 2011;38(2):656–67.
35. Hertanto A, Zhang Q, Hu Y, et al. Reduction of Irregular breathing artifacts in respiration-correlated CT images using a respiratory motion model. *Med Phys*. 2012;39(6):3070–79.
36. Lu W, Parikh PJ, Hubenschmidt JP, Bradley JD, Low DA. A comparison between amplitude sorting and phase-angle sorting using external respiratory measurement for 4D CT. *Med Phys*. 2006;33(8):2964–74.
37. Langner UW and Keall PJ. Accuracy in the localization of thoracic and abdominal tumors using respiratory displacement, velocity, and phase. *Med Phys*. 2009;36(2):386–93.
38. Schreibmann E, Chen GT, Xing L. Image interpolation in 4D CT using a BSpline deformable registration model. *Int J Radiat Oncol Biol Phys*. 2006;64(5):1537–50.
39. Guckenberger M, Weininger M, Wilbert J, et al. Influence of retrospective sorting on image quality in respiratory correlated computed tomography. *Radiother Oncol*. 2007;85(2):223–31.
40. Han D, Bayouth J, Song Q, Bhatia S, Sonka M, Wu X. Feature guided motion artifact reduction with structure-awareness in 4D CT images. *Proc IEEE Comput Soc Conf Comput Vis Pattern Recognit*, 2011. IEEE. 2011;1057–64.
41. Yen EK and Johnston RG. The ineffectiveness of the correlation coefficient for image comparisons. *J Phys Security*. 2007;2(1).
42. Olsen JR, Lu W, Hubenschmidt JP, et al. Effect of novel amplitude/phase binning algorithm on commercial four-dimensional computed tomography quality. *Int J Radiat Oncol Biol Phys*. 2008;70(1):243–52.
43. Langner UW and Keall PJ. Quantification of artifact reduction with real-time ciné four-dimensional computed tomography acquisition methods. *Int J Radiat Oncol Biol Phys*. 2010;76(4):1242–50.
44. Zhang Y, Yang J, Zhang L, Court LE, Balter PA, Dong L. Modeling respiratory motion for reducing motion artifacts in 4D CT images. *Med Phys*. 2013;40(4):041716.
45. Langner UW and Keall PJ. Prospective displacement and velocity-based ciné 4D CT. *Med Phys*. 2008;35(10):4501–12.
46. Coolens C, Bracken J, Driscoll B, Hope A, Jaffray D. Dynamic volume vs respiratory correlated 4DCT for motion assessment in radiation therapy simulation. *Med Phys*. 2012;39(5):2669–81.
47. Persson GF, Nygaard DE, Munck Af Rosenschold P, et al. Artifacts in conventional computed tomography (CT) and free breathing four-dimensional CT induce uncertainty in gross tumor volume determination. *Int J Radiat Oncol Biol Phys*. 2011;80(5):1573–80.
48. Mori S, Endo M, Komatsu S, Yashiro T, Kandatsu S, Baba M. Four-dimensional measurement of lung tumor displacement using 256-multi-slice CT-scanner. *Lung Cancer*. 2007;56(1):59–67.
49. Mori S, Hara R, Yanagi T, et al. Four-dimensional measurement of intrafractional respiratory motion of pancreatic tumors using a 256 multi-slice CT scanner. *Radiother Oncol*. 2009;92(2):231–37.
50. Wink N, Panknin C, Solberg TD. Phase versus amplitude sorting of 4D-CT data. *J Appl Clin Med Phys*. 2006;7(1):77–85.